

Asymptotically Stable Data-Driven Koopman Operator Approximation with Inputs using Total Extended DMD

Louis Lortie and James Richard Forbes

Department of Mechanical Engineering, McGill University
817 Sherbrooke Street West, Montreal QC H3A 0C3

Abstract

The Koopman operator framework can be used to identify a data-driven model of a nonlinear system. Unfortunately, when the data is corrupted by noise, the identified model can be biased. Additionally, depending on the choice of lifting functions, the identified model can be unstable, even when the underlying system is asymptotically stable. This paper presents an approach to reduce the bias in an approximate Koopman model, and simultaneously ensure asymptotic stability, when using noisy data. Additionally, the proposed data-driven modeling approach is applicable to systems with inputs, such as a known forcing function or a control input. Specifically, bias is reduced by using a total least-squares, modified to accommodate inputs in addition to lifted inputs. To enforce asymptotic stability of the approximate Koopman model, linear matrix inequality constraints are augmented to the identification problem. The performance of the proposed method is then compared to the well-known extended dynamic mode decomposition method and to the newly introduced forward-backward extended dynamic mode decomposition method using a simulated Duffing oscillator dataset and experimental soft robot arm dataset.

1 Introduction

Dynamic models of physical systems are used for many tasks, such as prediction, sensitivity analysis to initial conditions or parameter variation, and design. For complex systems, data-driven approaches to modeling [1, 2, 3, 4, 5, 6] are an attractive alternative to first-principles modeling, since a model structure can be assumed and then data is used to fit model parameters. The Koopman operator [7, 8, 4, 9] is becoming a popular modeling approach owing to its ability to represent a nonlinear system as an infinite-dimensional linear system. When working directly with data, the Koopman operator can be approximated, leading to a finite-dimensional approximate Koopman model [10, 11]. The lifting functions associated with the approximate Koopman model must be able to represent a rich enough set of nonlinearities in order to accurately describe the nonlinear behavior of the system. Depending on whether there are many lifting functions or many snapshots of the data, the Koopman operator is approximated using dynamic mode decomposition (DMD) [12, 13] or using extended DMD (EDMD) [8], respectively. An approximate Koopman model can then easily be represented as a state-space system [2], which can be used for other tasks, such as prediction [3, 14], stability analysis [15], or control design [16, 17, 9].

Identifying a real system from data involves measurements, and measurements are always corrupted by some amount of noise. When a dynamic model is fit using noisy data, the data-driven dynamic model can be biased [18, 19]. The bias in the Koopman operator approximation is reflected in the dynamics and input matrices. The bias can impact the eigenvalues of the dynamics matrix, resulting in eigenvalues that are shifted towards the origin of the complex plane, resulting in higher than expected decay rates [18]. Many papers in the literature provide methods to reduce the bias in the dynamics matrix, such as forward-backward DMD (fbDMD) [18] and total DMD (TDMD) [20, 19]. Recent work [21] has adapted fbDMD to also account for the bias in the input matrix, but there is no equivalent adaptation for the input matrix using TDMD. Extending TDMD to reduce the bias in the input matrix has the potential to outperform [21], since the authors in [18] show that TDMD reduces the bias more than fbDMD in the dynamics matrix. Additionally, when identifying an inherently asymptotically stable system, the resulting model can be unstable if the lifting functions are chosen poorly. If the underlying dynamics are asymptotically stable, then the data-driven model must be asymptotically stable as well, else the data-driven model is not at all representative of the true system and is not useful for tasks such as prediction. Some work from the literature provides constraints formulated as

linear matrix inequality (LMI) in the Koopman operator approximation problem to enforce asymptotic stability in the Koopman least-squares problem [22] and in the Koopman fbEDMD problem [21].

TDMD [19], inspired by total least-squares DMD [20, 23], projects the snapshot matrices onto an augmented matrix to reduce the bias in the dynamics matrix. This method is different than classic least squares, since it minimizes the orthogonal distance between the linear fit and the data points, while least squares minimizes the vertical distance between the linear fit and the data points [19]. This paper proposes a method to extend the application of TDMD to include both the dynamics and the input matrices associated with the approximate Koopman model. Including inputs to the TDMD framework allows for the consideration of a wider range of applications, such as regulated systems and engineering applications requiring inputs. Additionally, to ensure that the proposed method identifies an asymptotically stable Koopman system with reduced bias, this paper introduces a new formulation of the TDMD problem using LMI constraints to enforce asymptotic stability. In summary, the proposed method is a two-part method, which firstly projects the snapshot matrices with inputs onto an augmented matrix, and secondly computes the Koopman matrix with reduced bias by solving a convex optimization problem that imposes asymptotic stability on the identified system. The performance of the proposed method is compared to the state-of-the-art methods, forward-backward EDMD (fbEDMD) [21] and EDMD [8], using a simulated dataset of a Duffing oscillator and an experimental dataset of a soft robot arm.

1.1 Related work

The stochastic nature of sensor noise creates difficulties when employing system identification methods with noisy data. Some work in the literature proposes methods to mitigate the impact of noise on the dynamics matrix [24, 19, 18]. In [18], fbDMD is introduced as a method to leverage the forward- and backward-in-time dynamics of a system to reduce the bias in the eigenvalues of the dynamics matrix. Expanding on [18], the authors in [21] introduce fbEDMD to also reduce the bias in the input matrix. An additional method to reduce bias in the dynamics matrix of the Koopman system is TDMD [19]. TDMD is a two-step procedure in which 1) the snapshot matrices are projected on an augmented snapshot matrix, and then 2) the Koopman operator is approximated by solving a least-squares problem with the projected snapshot matrices. Although sensor noise can be characterized by various distributions, such as a Gaussian distribution, other types of disturbances such as outliers in the data can be complex to address. In [25], outlier rejection is performed by solving for weights based on a loss function.

An inherently asymptotically stable system can be identified as an unstable Koopman system if the lifting functions are chosen poorly. Additionally, in some cases, noise in the data can also result in the identification of an unstable Koopman system, even when the underlying system is asymptotically stable [26]. In order for the dynamic model to be as representative as possible, system identification methods should enforce asymptotic stability when required. In [27, 22], the authors enforce asymptotic stability on the approximate Koopman system by formulating the Koopman approximation problem as a series of LMI and bilinear matrix inequality (BMI) constraints. To formulate the Koopman operator approximation problem as a convex optimization problem, the BMI constraints used to enforce asymptotic stability on the Koopman system are transformed into a set of LMI constraints in [21] by using the method proposed in [28, 21, 29, 30]. In this paper, the Koopman operator approximation problem is formulated as a series of LMIs to enforce asymptotic stability leveraging the approach taken in [22, 21].

1.2 Contributions

This paper presents a new approximate Koopman modeling method, based on TDMD, that 1) reduces the bias in the dynamics and input matrices and 2) enforces asymptotic stability on the approximate Koopman system. The goal of this method is to identify an asymptotically stable Koopman representation with reduced bias when using noisy data regardless of the choice of lifting functions.

This paper derives the proposed method, *total EDMD with inputs and asymptotic stability constraint*, and validates it against EDMD [8], EDMD with an asymptotic stability constraint [27], fbEDMD [21], fbEDMD with an asymptotic stability constraint [21], and total EDMD with inputs using a simulated dataset of a Duffing oscillator and an experimental dataset of a soft robot arm.

1.3 Organization

This paper is organized in the following way. A review of pertinent background theory relevant to the proposed method is presented in Section 2. The proposed method is derived in Section 3 and formulated as a convex optimization problem in Section 4. Results using simulated and experimental datasets are presented in Section 5, and concluding remarks are given in Section 6.

2 Background theory

2.1 Dynamic mode decomposition

DMD [12] is a data-driven method used to reconstruct the dynamics of a system. In particular, DMD is useful when the system under investigation is complex and high-dimensional in features [2, 13]. Consider the dataset $\mathcal{D} = \{\mathbf{x}_k\}_{k=0}^m$ with snapshot matrices

$$\mathbf{X} = [\mathbf{x}_0 \quad \mathbf{x}_1 \quad \cdots \quad \mathbf{x}_{m-1}] \in \mathbb{R}^{n \times m}, \quad (1)$$

and

$$\mathbf{X}_+ = [\mathbf{x}_1 \quad \mathbf{x}_2 \quad \cdots \quad \mathbf{x}_m] \in \mathbb{R}^{n \times m}, \quad (2)$$

where $\mathbf{x}_k \in \mathbb{R}^{n \times 1}$ is a vector of the system's states. The subscript k represents the timestep such that $\mathbf{x}_k = \mathbf{x}(t_k)$ where $k = 0, 1, 2, \dots, m$. The best-fit matrix \mathbf{A} , where

$$\mathbf{X}_+ = \mathbf{A}\mathbf{X}, \quad (3)$$

advances the snapshot matrix in (1) by one time step. The matrix \mathbf{A} is the approximation of the dynamics matrix of the system. Solving (3) is equivalent to solving the least-squares problem

$$\mathbf{A} = \arg \min_{\mathbf{A}^*} \|\mathbf{X}_+ - \mathbf{A}^*\mathbf{X}\|_F^2, \quad (4)$$

whose solution is

$$\mathbf{A} = \mathbf{X}_+\mathbf{X}^\dagger, \quad (5)$$

where $(\cdot)^\dagger$ is the Moore-Penrose pseudoinverse. The objective of DMD is to find the leading eigendecomposition of \mathbf{A} when \mathbf{A} itself is too computationally demanding to compute or too large to store. Consider the SVD of the snapshot matrix

$$\mathbf{X} = \mathbf{W}\mathbf{\Sigma}\mathbf{V}^\top, \quad (6)$$

where $\mathbf{W} \in \mathbb{R}^{n \times n}$, $\mathbf{\Sigma} \in \mathbb{R}^{n \times m}$, and $\mathbf{V} \in \mathbb{R}^{m \times m}$. It follows that (5) can be written as

$$\mathbf{A} = \mathbf{X}_+\mathbf{V}\mathbf{\Sigma}^\dagger\mathbf{W}^\top. \quad (7)$$

Assume that the dynamics described by (3) have a low-dimensional structure. Truncating the singular values in (7) captures the main low-dimensional modes [2] while removing unwanted high-dimensional features. In turn, truncating the smaller singular values improves the conditioning of the pseudo-inverse in (5). After truncation, (7) is rewritten as

$$\mathbf{A} = \mathbf{X}_+\tilde{\mathbf{V}}\tilde{\mathbf{\Sigma}}^{-1}\tilde{\mathbf{W}}^\top, \quad (8)$$

where $\tilde{\mathbf{W}} \in \mathbb{R}^{n \times r}$, $\tilde{\mathbf{\Sigma}} \in \mathbb{R}^{r \times r}$, $\tilde{\mathbf{V}} \in \mathbb{R}^{r \times m}$, and r is the number of remaining singular values. When considering the case where $n \gg r$, it is more computationally efficient to compute $\tilde{\mathbf{A}}$, the projection of the dynamics matrix \mathbf{A} on the left singular vectors $\tilde{\mathbf{W}}$ as [2, 13]

$$\tilde{\mathbf{A}} = \tilde{\mathbf{W}}^\top\mathbf{A}\tilde{\mathbf{W}} = \tilde{\mathbf{W}}^\top\mathbf{X}_+\tilde{\mathbf{V}}\tilde{\mathbf{\Sigma}}^{-1}. \quad (9)$$

Note that the eigenvalues of $\tilde{\mathbf{A}}$ and \mathbf{A} are the same and that the eigenvectors of \mathbf{A} can be recovered as

$$\phi = \mathbf{X}_+\tilde{\mathbf{V}}\tilde{\mathbf{\Sigma}}^{-1}\mathbf{q}, \quad (10)$$

where \mathbf{q} is an eigenvector of $\tilde{\mathbf{A}}$. DMD is useful for studying the growth and decay rates, and the dynamic modes, of high-dimensional systems. Note that since DMD is used with (3), which describes the dynamics of a linear system, DMD can be used in tandem with Koopman operator theory to represent nonlinear systems as approximate linear systems. Additionally, DMDc is a method presented in [13] to perform DMD on a dataset with inputs.

2.2 Koopman operator theory

Consider a system whose discrete-time dynamics are governed by the nonlinear difference equation

$$\mathbf{x}_{k+1} = \mathbf{f}(\mathbf{x}_k, \mathbf{u}_k), \quad (11)$$

where $\mathbf{x}_k \in \mathcal{N} \subseteq \mathbb{R}^{n \times 1}$, $\mathbf{u}_k \in \mathcal{M} \subseteq \mathbb{R}^{m \times 1}$, and $\mathbf{f} : \mathbb{R}^{n \times 1} \times \mathbb{R}^{m \times 1} \rightarrow \mathbb{R}^{n \times 1}$. The Koopman operator $\mathcal{U} : \mathcal{H} \rightarrow \mathcal{H}$, which operates in the Hilbert space \mathcal{H} of infinitely many lifting functions $\psi : \mathcal{N} \times \mathcal{M} \rightarrow \mathbb{R}$, advance such lifting functions forward in time [2, 22] as

$$(\mathcal{U}\psi)(\mathbf{x}_k, \mathbf{u}_k) = \psi(\mathbf{x}_{k+1}, *), \quad (12)$$

where $* = \mathbf{u}_k$ or $* = \mathbf{0}$ if inputs of the system depend on the states of the system or if they do not, respectively. In practice, the Koopman operator is approximated using a finite number of lifting functions partitioned as

$$\psi(\mathbf{x}_k, \mathbf{u}_k) = \begin{bmatrix} \vartheta(\mathbf{x}_k) \\ \mathbf{v}(\mathbf{x}_k, \mathbf{u}_k) \end{bmatrix}, \quad (13)$$

where $\psi : \mathcal{M} \times \mathcal{N} \rightarrow \mathbb{R}^{p \times 1}$, $\vartheta : \mathcal{M} \rightarrow \mathbb{R}^{p_\vartheta \times 1}$, $\mathbf{v} : \mathcal{M} \times \mathcal{N} \rightarrow \mathbb{R}^{p_v \times 1}$, and $p = p_\vartheta + p_v$. The approximated Koopman operator then advances the finite number of lifting functions as

$$\vartheta(\mathbf{x}_{k+1}) = \mathbf{U}\psi(\mathbf{x}_k, \mathbf{u}_k) + \mathbf{r}_k, \quad (14)$$

where the residual \mathbf{r}_k exists due to the Koopman operator being approximated. The Koopman matrix is defined as

$$\mathbf{U} = \begin{bmatrix} \mathbf{A} & \mathbf{B} \end{bmatrix}, \quad (15)$$

which is an approximation of the Koopman operator in finite dimensions, and can be substituted into (14) to obtain the state-space representation

$$\vartheta(\mathbf{x}_{k+1}) = \mathbf{A}\vartheta(\mathbf{x}_k) + \mathbf{B}\mathbf{v}(\mathbf{x}_k, \mathbf{u}_k) + \mathbf{r}_k, \quad (16)$$

which evolves in the lifted space.

When the vector-valued lifting function $\mathbf{v}(\cdot)$ acts only on the inputs \mathbf{u}_k , then the dynamics matrix \mathbf{A} and input matrix \mathbf{B} respectively describe the evolution of the lifted states and lifted inputs of the system. The dynamics can then be rewritten as

$$\vartheta(\mathbf{x}_{k+1}) = \mathbf{A}\vartheta(\mathbf{x}_k) + \mathbf{B}\mathbf{v}(\mathbf{u}_k) + \mathbf{r}_k. \quad (17)$$

The systems of interest in this paper are described by the linear dynamics in (17) and the measurement equation

$$\zeta_k = \mathbf{C}\vartheta_k + \mathbf{D}\mathbf{v}_k + \mathbf{v}_k, \quad (18)$$

where, in this paper, \mathbf{v}_k represents a vector of white sensor noise, $\zeta_k \in \mathbb{R}^{p_\zeta \times 1}$, $\mathbf{C} = \mathbf{1}$, and $\mathbf{D} = \mathbf{0}$.

Let measurements collected from sensors and the inputs to the system over time steps $k = 0, 1, \dots, q$ be lifted and arranged into the snapshot matrices

$$\Psi = [\psi_0 \quad \psi_1 \quad \cdots \quad \psi_{q-1}] \in \mathbb{R}^{p \times q}, \quad (19)$$

and

$$\Theta_+ = [\vartheta_1 \quad \vartheta_2 \quad \cdots \quad \vartheta_q] \in \mathbb{R}^{p_\vartheta \times q}, \quad (20)$$

where $\psi_k = \psi(\mathbf{x}_k, \mathbf{u}_k)$ and $\vartheta_k = \vartheta(\mathbf{x}_k)$. Using (19) and (20), the Koopman matrix is computed by solving the least-squares problem

$$\mathbf{U} = \arg \min_{\mathbf{U}^*} \|\Theta_+ - \mathbf{U}^* \Psi\|_{\mathbb{F}}^2, \quad (21)$$

giving the solution [2]

$$\mathbf{U} = \Theta_+ \Psi^\dagger, \quad (22)$$

where $\|\cdot\|_{\mathbb{F}}$ is the Frobenius norm. When $q \gg p$, then it is preferred to compute the Koopman matrix using EDMD [8] in order to reduce the size of the pseudoinverse problem on Ψ , such that (22) becomes

$$\mathbf{U} = \Theta_+ \Psi^\dagger = (\Theta_+ \Psi^\top)(\Psi \Psi^\top)^\dagger = \mathbf{G}\mathbf{H}^\dagger, \quad (23)$$

where

$$\mathbf{G} = \frac{1}{q} \Theta_+ \Psi^\top \in \mathbb{R}^{p_\vartheta \times p}, \quad \mathbf{H} = \frac{1}{q} \Psi \Psi^\top \in \mathbb{R}^{p \times p}, \quad (24)$$

and q is the number of snapshots.

3 Total DMD with inputs

In practice, data collected from real systems is corrupted by noise that can lead to a bias in the identified model. DMD and the standard least-squares problem do not mitigate the effect of noise in the identification process of the Koopman matrix. In [13], TDMD, which is a version of DMD inspired by total least-squares, is introduced to reduce the effect of noise by using a projection step before computing the Koopman matrix with least squares. However, TDMD is only used with datasets that consist of collected measurements and no inputs.

In this section, the existing TDMD method is reviewed and then modified to accommodate inputs. The proposed method, TDMD with inputs (TEDMD), does not only reduce the bias found in the dynamics matrix, but also reduces the bias in the input matrix.

3.1 Total least-squares formulation of DMD

Consider a dynamical system with no inputs whose Koopman matrix is computed by solving the least-square problem

$$\mathbf{U} = \arg \min_{\mathbf{U}^*} \|\Theta_+ - \mathbf{U}^* \Theta\|_F^2. \quad (25)$$

The solution to (25) is

$$\mathbf{U} = \Theta_+ \Theta^\dagger, \quad (26)$$

where

$$\Theta = [\vartheta_0 \quad \vartheta_1 \quad \cdots \quad \vartheta_{q-1}] \in \mathbb{R}^{p\vartheta \times q}, \quad (27)$$

and Θ_+ is defined by (20). The solution in (26) to the least-squares problem in (25) is computed under the assumption that the noise corrupting the data is only present in Θ_+ . Specifically, the least-squares problem in (25) is equivalent to

$$\min J(\mathbf{U}_{\text{ls}}, \mathbf{N}_{\Theta_+}) = \|\mathbf{N}_{\Theta_+}\|_F \quad (28)$$

$$\text{s.t. } \Theta_+ + \mathbf{N}_{\Theta_+} = \mathbf{U}_{\text{ls}} \Theta, \quad (29)$$

where \mathbf{N}_{Θ_+} is the added noise to Θ_+ . This one-sided assumption creates a bias in the identified Koopman matrix. Total least-squares addresses this problem by assuming that noise is present in both snapshot matrices, such that the problem in (28) and (29) becomes [19]

$$\min J(\mathbf{U}_{\text{tls}}, \mathbf{N}_{\Theta}, \mathbf{N}_{\Theta_+}) = \left\| \begin{bmatrix} \mathbf{N}_{\Theta} \\ \mathbf{N}_{\Theta_+} \end{bmatrix} \right\|_F \quad (30)$$

$$\text{s.t. } \Theta_+ + \mathbf{N}_{\Theta_+} = \mathbf{U}_{\text{tls}}(\Theta + \mathbf{N}_{\Theta}). \quad (31)$$

TDMD [19], which is inspired by total least-squares, involves a projection step and an identification step [19]. Consider the augmented matrix

$$\mathbf{Z} = \begin{bmatrix} \Theta \\ \Theta_+ \end{bmatrix}. \quad (32)$$

As opposed to regular least squares, TDMD does not only project Θ and Θ_+ on the range of Θ^\top , but on the range of \mathbf{Z}^\top , which captures both the range of Θ^\top and Θ_+^\top . Consider the SVD

$$\mathbf{Z} = \mathbf{W} \Sigma \mathbf{V}^\top, \quad (33)$$

where $\mathbf{W} \in \mathbb{R}^{(p\vartheta+p\vartheta) \times r}$, $\Sigma \in \mathbb{R}^{r \times r}$, $\mathbf{V} \in \mathbb{R}^{q \times r}$. The transpose of \mathbf{Z} is given by

$$\mathbf{Z}^\top = \mathbf{V} \Sigma \mathbf{W}^\top. \quad (34)$$

Note that the SVD of either \mathbf{Z} or \mathbf{Z}^\top can be truncated. Throughout this paper, it's assumed the SVD of \mathbf{Z} is truncated. The projection matrix onto the range of \mathbf{Z}^\top is

$$\mathbb{P}_{\mathbf{Z}^\top} = \mathbf{V} \mathbf{V}^\top. \quad (35)$$

Then, let the snapshot matrices Θ and Θ_+ be projected onto the range of \mathbf{Z}^\top , such that the approximate Koopman dynamics become

$$\Theta_+ \mathbb{P}_{\mathbf{Z}^\top} = \mathbf{U}_{\text{tdmd}} \Theta \mathbb{P}_{\mathbf{Z}^\top}, \quad (36)$$

$$\bar{\Theta}_+ = \mathbf{U}_{\text{tdmd}} \bar{\Theta}, \quad (37)$$

where $\bar{\Theta} = \Theta \mathbb{P}_{\mathbf{Z}^\top}$ and $\bar{\Theta}_+ = \Theta_+ \mathbb{P}_{\mathbf{Z}^\top}$. Several methods are presented in the literature [31, 32, 33] to find the optimal singular value threshold at which to truncate the SVD in order to keep the main low-rank spatiotemporal features while removing less important features [2]. One method to obtain the optimal singular value threshold is the singular value hard threshold method introduced in [31]. In practice, for a shorter computing time, the snapshot matrices $\bar{\Theta} \in \mathbb{R}^{p_\theta \times q}$ and $\bar{\Theta}_+ \in \mathbb{R}^{p_\theta \times q}$ do not have to be explicitly used, since when the number of snapshots q is high, then solving for \mathbf{U}_{tdmd} in (37) becomes computationally demanding. Instead, the smaller matrices

$$\hat{\Theta} = \Theta \mathbf{V} \in \mathbb{R}^{p_\theta \times r}, \quad \hat{\Theta}_+ = \Theta_+ \mathbf{V} \in \mathbb{R}^{p_\theta \times r} \quad (38)$$

are computed to form [19]

$$\hat{\Theta}_+ = \mathbf{U}_{\text{tdmd}} \hat{\Theta}. \quad (39)$$

After the projection step taken in (38), the Koopman matrix is computed by solving the least-squares problem in (39), which results in

$$\mathbf{U}_{\text{tdmd}} = \hat{\Theta}_+ \hat{\Theta}^\dagger. \quad (40)$$

In this section, TDMD is introduced as a method that computes a Koopman matrix with reduced bias by first projecting the snapshot matrices onto the range of an augmented matrix and then computing the Koopman matrix by solving the least-squares problem in (40).

3.2 Modification of TDMD to include inputs

TDMD is presented as a two-step method that reduces the bias in the dynamics matrix through a projection step and an identification step. However, TDMD is a method that reduces the impact of noise when the dataset used for identification has no inputs. Next, a modification to TDMD, where inputs are considered in the TDMD framework to identify the dynamics and input matrices with reduced bias is proposed.

For a system with inputs, its dynamics and input matrices can be computed using the least-squares solution

$$[\mathbf{A}_{\text{ls}} \quad \mathbf{B}_{\text{ls}}] = \Theta_+ \Psi^\dagger, \quad (41)$$

where Θ_+ and Ψ are defined in (20) and (19), respectively. The formulation of the problem in (41) also assumes that noise is present only in Θ_+ . Therefore, an equivalent method to TDMD must be derived to consider noise in both matrices. As in Section 3.1, consider the augmented snapshot matrix

$$\mathbf{T} = \begin{bmatrix} \Psi \\ \Theta_+ \end{bmatrix}, \quad (42)$$

with SVD

$$\mathbf{T} = \mathbf{W} \Sigma \mathbf{V}^\top. \quad (43)$$

The projection matrix onto the range of \mathbf{T}^\top is

$$\mathbb{P}_{\mathbf{T}^\top} = \mathbf{V} \mathbf{V}^\top. \quad (44)$$

Then, let the snapshot matrices Ψ and Θ_+ be projected onto the range of \mathbf{T}^\top as

$$\Theta_+ \mathbb{P}_{\mathbf{T}^\top} = \mathbf{U}_{\text{tdmdc}} \Psi \mathbb{P}_{\mathbf{T}^\top}, \quad (45)$$

$$\bar{\Theta}_+ = \mathbf{U}_{\text{tdmdc}} \bar{\Psi}, \quad (46)$$

where $\bar{\Psi} = \Psi \mathbb{P}_{\mathbf{T}^\top}$ and $\bar{\Theta}_+ = \Theta_+ \mathbb{P}_{\mathbf{T}^\top}$.

Finally, the Koopman matrix with reduced bias identified from a dataset with inputs is computed with the least-squares solution

$$\mathbf{U}_{\text{tdmdc}} = \hat{\Theta}_+ \hat{\Psi}^\dagger, \quad (47)$$

where

$$\hat{\Psi} = \Psi \mathbf{V}, \quad \hat{\Theta}_+ = \Theta_+ \mathbf{V}. \quad (48)$$

The derivation for the TEDMD follows in parallel that of the TDMD. The difference lies in the construction of the augmented matrices described by (32) and (42). Although similar to TDMD, TEDMD allows for a much wider range of applications where noise corrupts data with inputs.

4 Formulation of the optimization problem

The Koopman operator approximation problem with TEDMD can be computed traditionally using (47) or equivalently as

$$\mathbf{U} = \arg \min_{\mathbf{U}^*} \left\| \left(\hat{\Theta}_+ - \mathbf{U}^* \hat{\Psi} \right) \Omega \right\|_F^2, \quad (49)$$

where Ω is a weight nominally set to the identity matrix. As highlighted in [21, 22], the Koopman operator optimization problem described by (49) can be formulated in a modular fashion as a series of LMIs. This feature allows the problem to be written in tandem with LMI constraints to enforce specific requirements on the Koopman matrix. For models of real systems, one potential requirement is asymptotic stability. In particular, any real system that is asymptotically stable must have a Koopman representation that is also asymptotically stable.

For a discrete-time system to be asymptotically stable, its dynamics matrix must have its eigenvalues bounded strictly within the unit circle [34]. To enforce asymptotic stability on the Koopman system with reduced bias, the BMI constraint [34, 22]

$$\begin{bmatrix} \bar{\rho} \mathbf{P} & \mathbf{A} \mathbf{P} \\ \star & \bar{\rho} \mathbf{P} \end{bmatrix} > 0, \quad (50)$$

with

$$\mathbf{P} > 0, \quad (51)$$

where \star defines the transpose of its off-diagonal counterpart and $\bar{\rho}$ is the spectral bound on the eigenvalues of \mathbf{A} , is added to the optimization problem in (49). In particular, the optimization problem is now

$$\mathbf{U} = \arg \min_{\mathbf{A}, \mathbf{B}, \mathbf{P}} \left\| \left(\hat{\Theta}_+ - [\mathbf{A} \ \mathbf{B}] \hat{\Psi} \right) \Omega \right\|_F^2 \quad (52)$$

$$\text{s.t. } \mathbf{P} > 0, \quad \begin{bmatrix} \bar{\rho} \mathbf{P} & \mathbf{A} \mathbf{P} \\ \star & \bar{\rho} \mathbf{P} \end{bmatrix} > 0. \quad (53)$$

Note that the optimization problem described in (52) and (53) is not convex because of the bilinear term $\mathbf{A} \mathbf{P}$. To transform the above nonconvex problem as a convex problem, the change of variable $\mathbf{F} = \mathbf{A} \mathbf{P}$ proposed in [28, 21, 29, 30] is used. Setting the weight Ω equal to

$$\Omega = \hat{\Psi}^\top (\hat{\Psi} \hat{\Psi}^\top)^\dagger \bar{\mathbf{P}}, \quad (54)$$

in (52) yields the convex optimization problem

$$\min J(\mathbf{F}, \mathbf{B}, \mathbf{P}) = \left\| \hat{\mathbf{G}} \hat{\mathbf{H}}^\dagger \bar{\mathbf{P}} - [\mathbf{F} \ \mathbf{B}] \right\|_F^2 \quad (55)$$

$$\text{s.t. } \mathbf{P} > \epsilon, \quad \begin{bmatrix} \bar{\rho} \mathbf{P} & \mathbf{F} \\ \star & \bar{\rho} \mathbf{P} \end{bmatrix} > 0, \quad (56)$$

where

$$\bar{\mathbf{P}} = \begin{bmatrix} \mathbf{P} & \mathbf{0} \\ \mathbf{0} & \mathbf{1} \end{bmatrix}, \quad (57)$$

$\hat{\mathbf{G}} = \hat{\Theta}_+ \hat{\Psi}^\top$, $\hat{\mathbf{H}} = \hat{\Psi} \hat{\Psi}^\top$, $\mathbf{F} = \mathbf{A} \mathbf{P}$, and ϵ is added to set a lower bound on \mathbf{P} in order to not let \mathbf{P} be prioritize when minimizing the cost function in (55). Then, a slack variable is introduced to decompose the cost function in (55) as a

combination of LMI constraints [35, 22, 21], such that the final optimization becomes

$$\min J(\gamma, \mathbf{F}, \mathbf{B}, \mathbf{P}, \hat{\mathbf{R}}) = \gamma \quad (58)$$

$$\text{s.t. } \text{tr}(\hat{\mathbf{R}}) < 1, \quad \hat{\mathbf{R}} > 0, \quad \begin{bmatrix} \hat{\mathbf{R}} & (\hat{\mathbf{G}}\hat{\mathbf{H}}^\top\bar{\mathbf{P}} - [\mathbf{F} \ \mathbf{B}])^\top \\ \star & \gamma\mathbf{1} \end{bmatrix} > 0, \quad (59)$$

$$\mathbf{P} > \epsilon, \quad \begin{bmatrix} \bar{\rho}\mathbf{P} & \mathbf{F} \\ \star & \bar{\rho}\mathbf{P} \end{bmatrix} > 0, \quad (60)$$

where \mathbf{A} can be solved for using $\mathbf{A} = \mathbf{F}\mathbf{P}^{-1}$. The Koopman matrix is then computed by solving the optimization problem in (58)–(60) where

$$\mathbf{U} = [\mathbf{A} \ \mathbf{B}]. \quad (61)$$

A detailed derivation from (49) to (60) is presented in [21].

In this section, the Koopman operator approximation problem is posed as a convex optimization problem with LMI constraints that enforce asymptotic stability on the system. Enforcing asymptotic stability is important, since the approximate Koopman representation of the asymptotically stable system must be properly representative.

5 Results and discussion

To validate that the proposed method, TDMD with inputs and asymptotic stability constraint (TEDMD-AS), solves for an asymptotically stable approximate Koopman system with reduced bias and, as will be shown, outperforms other state-of-the-art methods when testing using a simulated Duffing oscillator dataset and an experimental soft robot arm dataset. In this section, TEDMD-AS is compared to total DMD with inputs (TEDMD), EDMD, EDMD with an asymptotic stability constraint (EDMD-AS), forward-backward EDMD with inputs (fbEDMD), and forward-backward EDMD with inputs and asymptotic stability constraints (fbEDMD-AS) to assess its prediction and bias reduction performance. The methods using asymptotic stability are also compared to the methods that do not use constraints. The Koopman matrices identified from TEDMD and TEDMD-AS are computed using the optimization problem described in (49) and (58)–(60), respectively. EDMD-AS and fbEDMD-AS compute Koopman matrices using the optimization problems described in [21, §5]. As for EDMD, the Koopman matrix is generated by `pykoop` [36], an open-source Koopman operator identification library. Forward-backward EDMD uses `pykoop` and the method described in [21, §3.2]. All three methods with asymptotic stability constraints use the spectral radius bound $\bar{\rho} = 0.99999$ [21].

5.1 Simulation results

A simulated dataset of a Duffing oscillator is used to compare approximate Koopman systems generated by the different methods. In particular, the system that generates the dataset for this section is described by the ordinary differential equation

$$m\ddot{x}(t) + c\dot{x}(t) + k_1x(t) + k_2x(t)^3 = f(t), \quad (62)$$

where the mass $m = 0.1$ kg, damping coefficient $c = 0.01$ Ns/m, linear spring constant $k_1 = 0.1$ N/m and nonlinear spring constant $k_2 = 0.001$ N/m³. To generate the discretized dataset, Euler’s forward method [37, §6.1] is used. Additionally, this simulated dataset consists of 20 training episodes and 2 testing episodes. To lift the simulated data into the lifted space, the chosen lifting functions are all the different combinations of second-order monomials and ten radial basis functions of the form

$$\psi_i^{\text{rbf}}(\mathbf{x}) = r_i^2 \ln(r_i), \quad i = 1, \dots, 10, \quad (63)$$

where

$$r_i = \alpha \|\boldsymbol{\psi}^{\text{poly}}(\mathbf{x}) - \mathbf{c}_i\| + \delta, \quad (64)$$

$\boldsymbol{\psi}^{\text{poly}}(\mathbf{x})$ is a vector-valued lifting function made of all second-order monomial combinations, \mathbf{c}_i is a center generated by a Latin hypercube sampling algorithm [38, 39], $\alpha = 0.1$ is a parameter used to define the scaling, and $\delta = 0.001$ ensures that the computed number is defined. Note that the values for α and δ are tuned based on the dataset and chosen lifting functions to obtain the best fit. Additionally, the signal-to-noise ratio (SNR), computed as

$$\text{SNR} = 10 \log \left(\frac{\sigma_x^2}{\sigma_n^2} \right), \quad (65)$$

where σ_x is the standard deviation of the original signal and σ_n is the standard deviation of the added noise, is used to describe the amount of noise added to the original trajectory of the system. The added noise \mathbf{v}_k found in the measurement equation described by (18) is simulated by white noise of distribution $\mathbf{v}_k \sim \mathcal{N}(\mathbf{0}, \Sigma_v)$, where the covariance matrix Σ_v is set to obtain a particular SNR. In this paper, SNRs of 18 dB and 28 dB are evaluated, where 18 dB corresponds to more noise than 28 dB.

Before diving into the results of TEDMD, a particular challenge in the projection step of TEDMD must be discussed. When the left singular vectors of the augmented matrix are used to project the snapshot matrices in (36) of TEDMD, the condition number of both snapshot matrices Θ_+ and Ψ increases, making the least-squares problem in (49) have larger condition numbers than the regular least-squares problem in (21) [23]. A solution to this problem is to truncate the SVD problem as mentioned in Section 3.2. There exists a trade-off between removing too few or too many singular values to form \mathbf{V} described in (44). When truncating many singular values, the condition number of the projected matrices decreases, but some information contained in the original snapshot matrices is lost. On the other hand, keeping too many singular values leads to the solver finding no solution due to large condition numbers of the projected snapshot matrices. The optimal truncation value for \mathbf{V} must therefore be large enough to keep all the important singular vectors, while maintaining a low enough condition number to allow for a solution of the least-squares problem. Although the literature provides different methods, such as the hard threshold method [31] to select the optimal singular value at which truncation should occur, it was noticed that none of these methods would consistently generate the optimal truncation value for all the range of SNRs considered in this paper. Therefore, for all considered SNRs, the number of singular values to keep is individually hand-picked as the highest integer possible, while having a low enough condition number on both projected snapshot matrices to allow for a solution in the projected least-squares problem.

The ability of a method to enforce asymptotic stability on the computed Koopman system is assessed by observing if all of the eigenvalues of the system's dynamics matrix are within the unit circle of the complex plane. Note that the ability of a method with no asymptotic stability constraint to generate an asymptotic stability approximate Koopman system depends on many factors such as the dataset and the chosen lifting functions. In particular, just as EDMD-AS, fbEDMD-AS, and TEDMD-AS compute dynamics matrices with eigenvalues within the unit circle in Figure 1, EDMD also computes a dynamics matrix with all of its eigenvalues inside the unit circle. Consequently, for simplicity, when comparing trajectories generated from different identification methods, the trajectories of EDMD, fbEDMD and TEDMD are omitted as they can generate unstable trajectories, as shown from the eigenvalues in Figure 1.

A useful feature of dynamic models is to predict a system's response to a given set of initial conditions. Next, the approximate Koopman models computed by the different methods are used to compare trajectory prediction errors, where the smallest error corresponds to the approximate Koopman model that generated the closest trajectory to the true trajectory. To emphasize the ability of TEDMD-AS and fbEDMD-AS to reduce the bias in the system's trajectory in the presence of noise, Figure 2i and Figure 2ii show generated trajectories when the dataset used for identification has an SNR of 28 dB and 18 dB, respectively. The trajectory generated by the Koopman matrix computed with EDMD-AS in Figure 2i is shown to have a significant bias compared to the trajectories obtained with TEDMD-AS and fbEDMD-AS. In this case, the bias in the Koopman matrix is analogous to a bias in the eigenvalues, leading to a higher decay rate. When comparing fbEDMD-AS and TEDMD-AS at an SNR of 28 dB in Figure 2i, fbEDMD-AS has a lower error than TEDMD-AS. However, both fbEDMD-AS and TEDMD-AS have a reduced bias in their trajectories compared to EDMD-AS. When the dataset is corrupted by noise with an SNR of 18 dB, the trajectory generated with TEDMD-AS has a lower error than both fbEDMD-AS and EDMD-AS. It can therefore be said that above a certain threshold of noise, TEDMD-AS outperforms both EDMD-AS and fbEDMD-AS.

5.2 Experimental results

In this section, the different identification methods are tested with an experimental dataset of a soft robot arm [16, 17]. This soft robot arm is controlled by three pressure regulators, which act as this system's control inputs. The laser pointer mounted on the end effector of this soft robot points onto a board, where the x - y coordinates of the point represent this system's states and output measurement. The provided dataset consists of 13 training training episodes and 4 test episodes. Although all experimental datasets have some noise due to the noisy nature of sensors, additional white noise modeled as $\mathbf{w}_k \sim \mathcal{N}(\mathbf{0}, \Sigma_w)$ is added to the measurement equation in (18) to emphasize the ability to reduce the bias in the Koopman system due to noise for TEDMD methods. Similarly to the simulated dataset, the covariance matrix Σ_w is set so that the experimental dataset with added noise has a specific SNR. In this section,

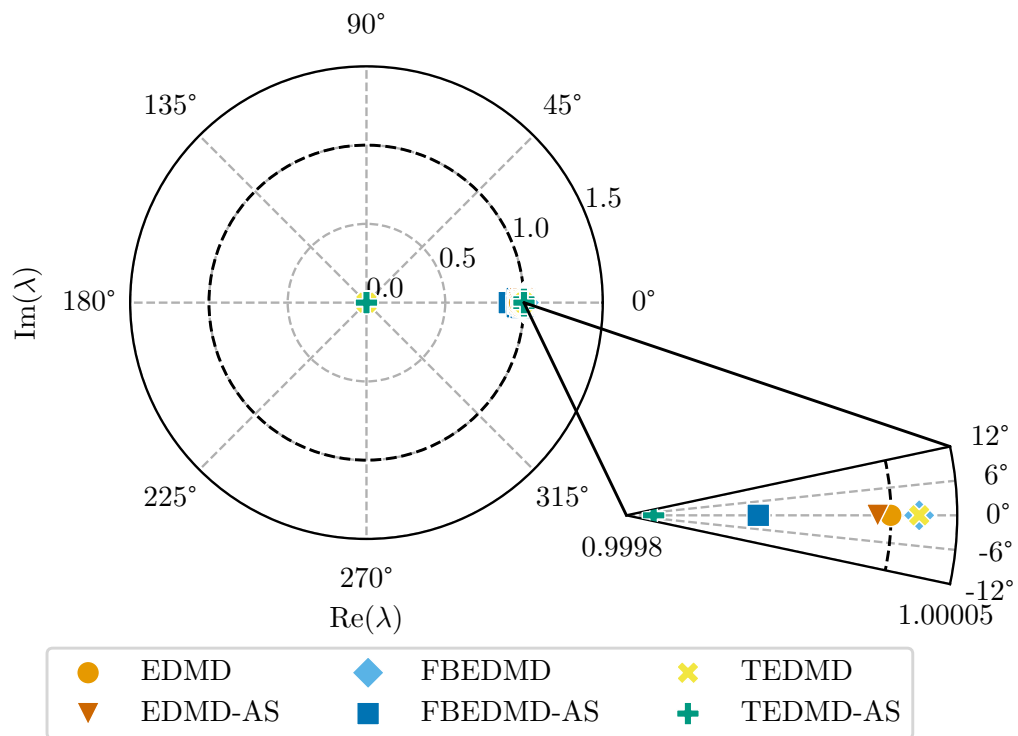
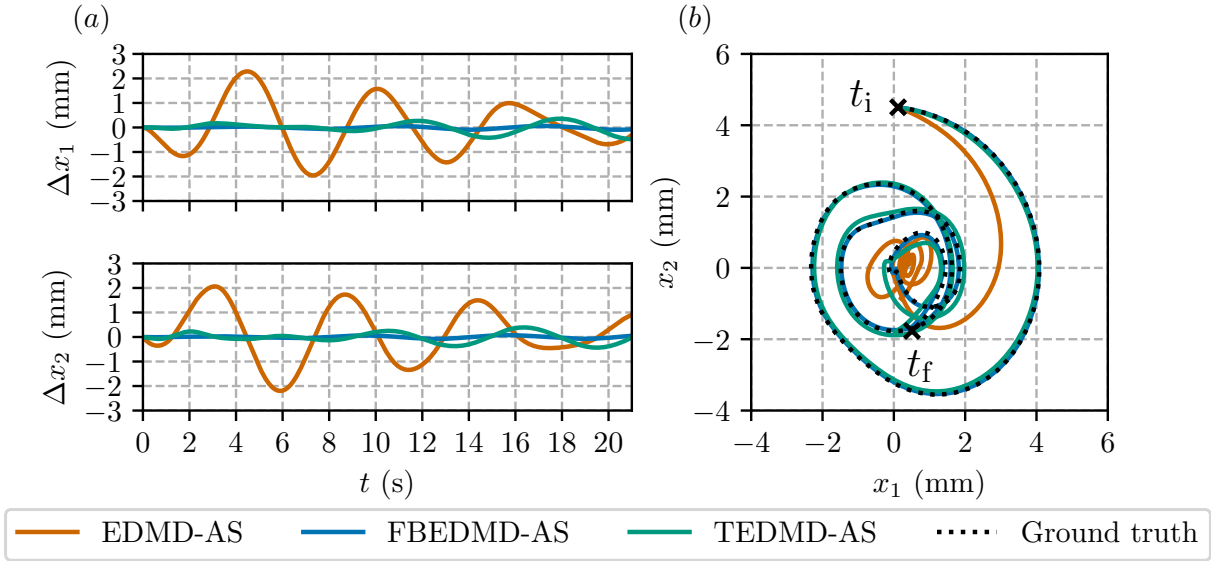
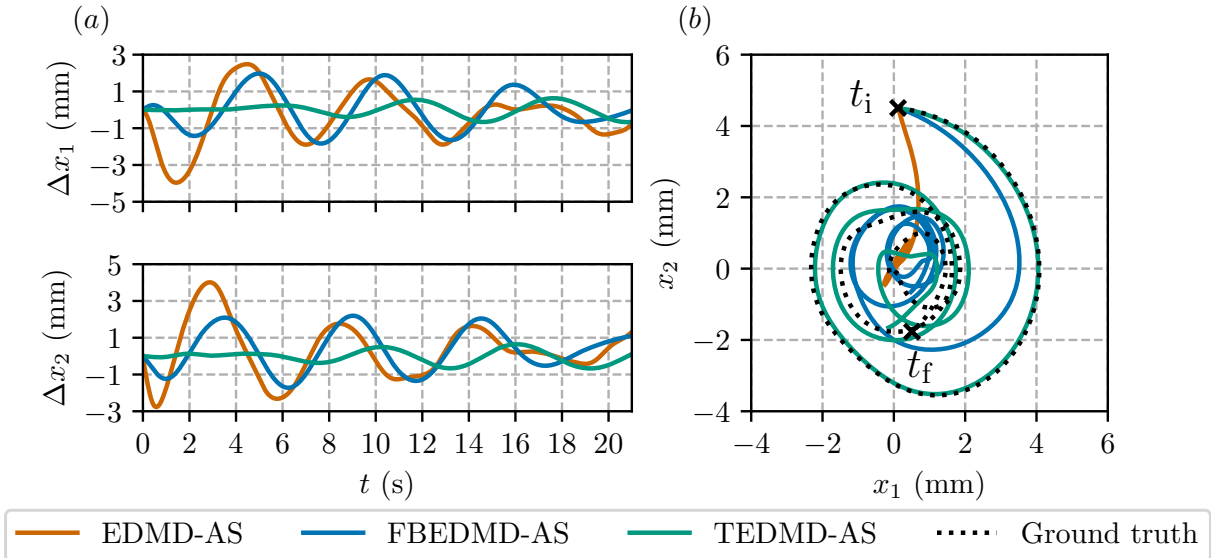


Figure 1: Eigenvalues of the identified Koopman matrices using the simulated Duffing oscillator dataset at an SNR of 28 dB. All the methods with asymptotic stability constraints, EDMD-AS, fbEDMD-AS, and TEDMD-AS, have their largest eigenvalue bounded strictly within the unit circle, which means that the identified Koopman systems are asymptotically stable. Forward-backward EDMD and TEDMD produce unstable systems with some eigenvalues of the Koopman matrices outside the unit circle. Although EDMD does not enforce asymptotic stability, it still identified a stable Koopman system.



(i) Prediction error plot (a) and multi-step trajectory (b) for Koopman matrices identified with an SNR of 28 dB. The trajectory generated by the Koopman matrix identified with EDMD-AS exhibits a large bias compared to fbEDMD-AS and TEDMD-AS, which is reflected by larger decay rates. While both fbEDMD-AS and TEDMD-AS identify Koopman matrices that predict the trajectory with a low error, fbEDMD-AS shows a lower error than TEDMD-AS.



(ii) Prediction error plot (a) and multi-step trajectory (b) for Koopman matrices identified with an SNR of 18 dB. The trajectory generated by the Koopman matrix identified with EDMD-AS exhibits a large bias compared to fbEDMD-AS and TEDMD-AS, which is reflected by larger decay rates. Compared to TEDMD-AS, fbEDMD-AS identifies a Koopman matrix with a higher bias. The Koopman matrix identified with TEDMD-AS predicts the trajectory with the lowest error.

Figure 2: Prediction error plots and multi-step trajectories of the first test episode for all three asymptotically stable Koopman systems identified with the simulated Duffing oscillator dataset at an SNR of (i) 28 dB and (ii) 18 dB. At each step of the prediction, the states are recovered and re-lifted. The prediction starts at $t_i = 0$ s and finishes at $t_f = 21$ s.

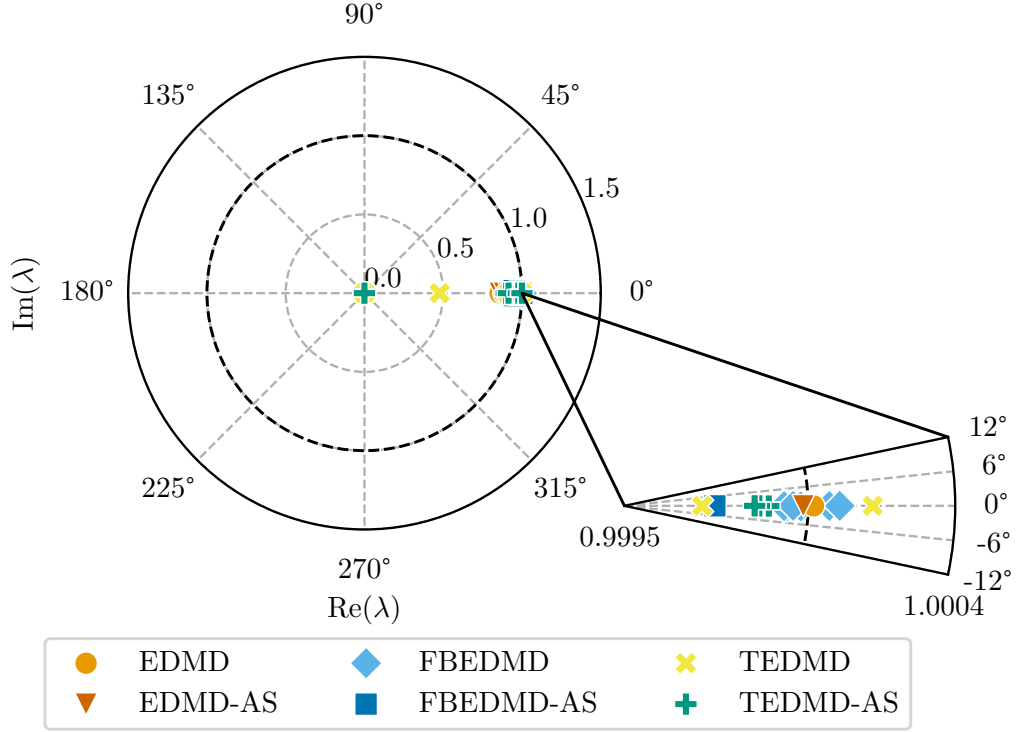


Figure 3: Eigenvalues of the identified Koopman matrices using the experimental soft robot arm dataset at an SNR of 28 dB. All the methods with asymptotic stability constraints, EDMD-AS, fbEDMD-AS, and TEDMD-AS, have their largest eigenvalue bounded strictly within the unit circle, which means that the identified Koopman systems are asymptotically stable. Extended DMD, fbEDMD, and TEDMD produce unstable systems with some eigenvalues of the Koopman matrices outside the unit circle.

the concept of *true* Koopman matrix is discussed. The true Koopman matrix refers to the Koopman matrix identified with the original dataset without added noise as opposed to the predicted Koopman matrix, which is the Koopman matrix identified with the added noise. The lifting functions used to fit the Koopman model to the data are the same as described in Section 5.1, but with a shape factor $\alpha = 0.5$.

The effect of adding asymptotic stability constraints to the approximate Koopman identification problem is demonstrated in Figure 3, where EDMD, fbEDMD, and TEDMD have eigenvalues located outside the unit circle. Consequently, Koopman systems obtained with EDMD, fbEDMD, and TEDMD are unstable and therefore will not be used for trajectory prediction, since the predictions will eventually diverge to infinity. When asymptotic stability constraints are used, as with EDMD-AS, fbEDMD-AS, and TEDMD-AS, all eigenvalues of the computed approximate Koopman matrices are strictly within the unit circle. Note that EDMD identified a Koopman matrix with eigenvalues outside the unit circle in Figure 3, but not in Figure 1, which shows that asymptotic stability constraints are important in order to have all eigenvalues within the unit circle.

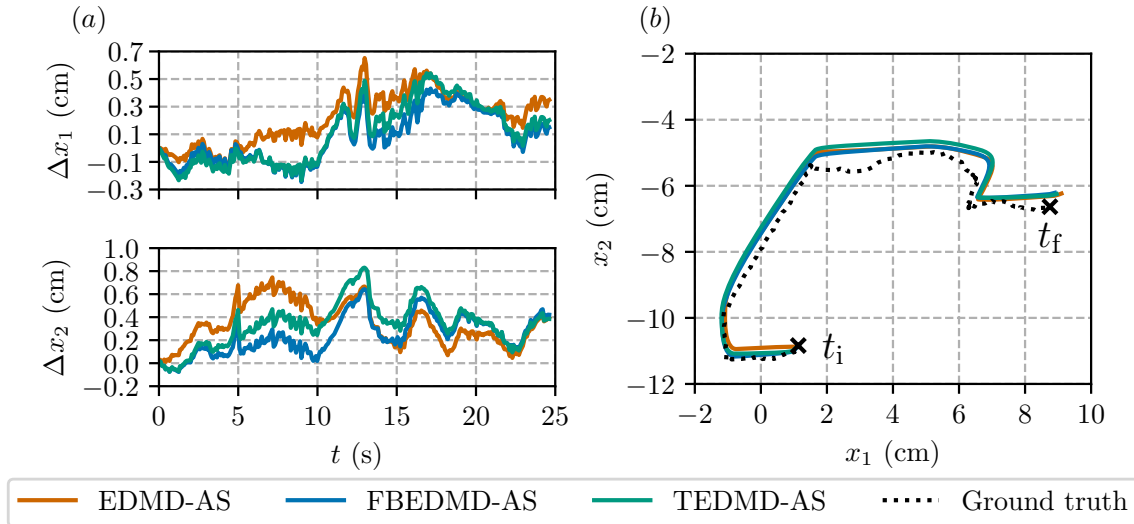
When predicting trajectories of the soft robot arm, as shown in Figure 4i, there is no clear best method, since EDMD-AS, fbEDMD-AS, and TEDMD-AS all have similar errors. Therefore, to compare prediction performances, the mean absolute error (MAE), and root-mean-square error (RMSE) are used as metrics, where [40]

$$\text{MAE} = \frac{\sum_{k=1}^q \|\mathbf{x}_k - \hat{\mathbf{x}}_k\|_1}{q}, \quad (66)$$

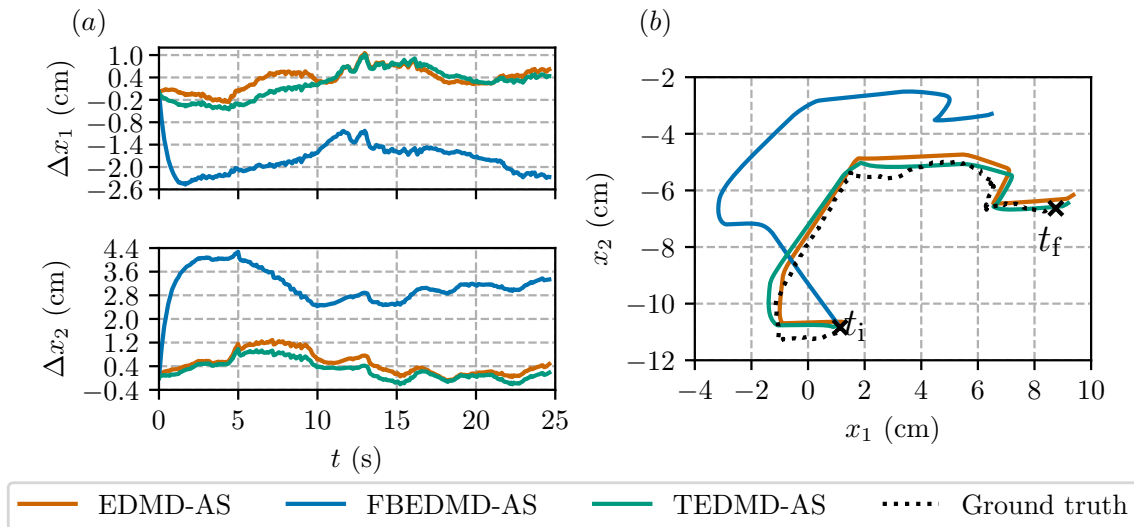
$$\text{RMSE} = \sqrt{\frac{\sum_{k=1}^q \|\mathbf{x}_k - \hat{\mathbf{x}}_k\|_2^2}{q}}, \quad (67)$$

\mathbf{x}_k is the ground truth of the trajectory at time step k , and $\hat{\mathbf{x}}_k$ is the predicted trajectory at time step k . The RMSE is chosen as an error metric because it measures the dispersion of the predicted trajectory around the ground truth, while

MAE is picked as another error metric since it represents the bias in the error [41]. In Figure 5i, when the dataset has an SNR of 28 dB, TEDMD-AS has a higher averaged root-mean-square and mean error than both EDMD-AS and fbEDMD-AS. As for fbEDMD-AS, it generates a trajectory with a higher root-mean-square error, but lower mean error than EDMD-AS. From the results, TEDMD-AS does not perform better than EDMD-AS or fbEDMD-AS in terms of predictions when the soft robot arm dataset has an SNR of 28 dB.

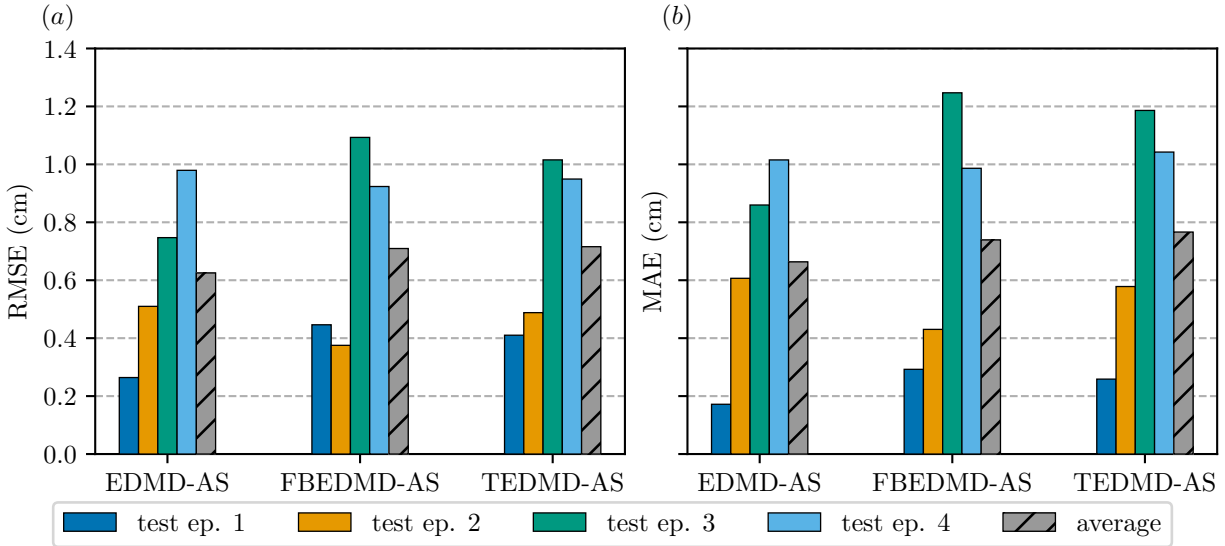


(i) Prediction error plot (a) and multi-step trajectory (b) for Koopman matrices identified with an SNR of 28 dB. All three Koopman matrices identified with EDMD-AS, fbEDMD-AS, and TEDMD-AS predict trajectories with similar errors.

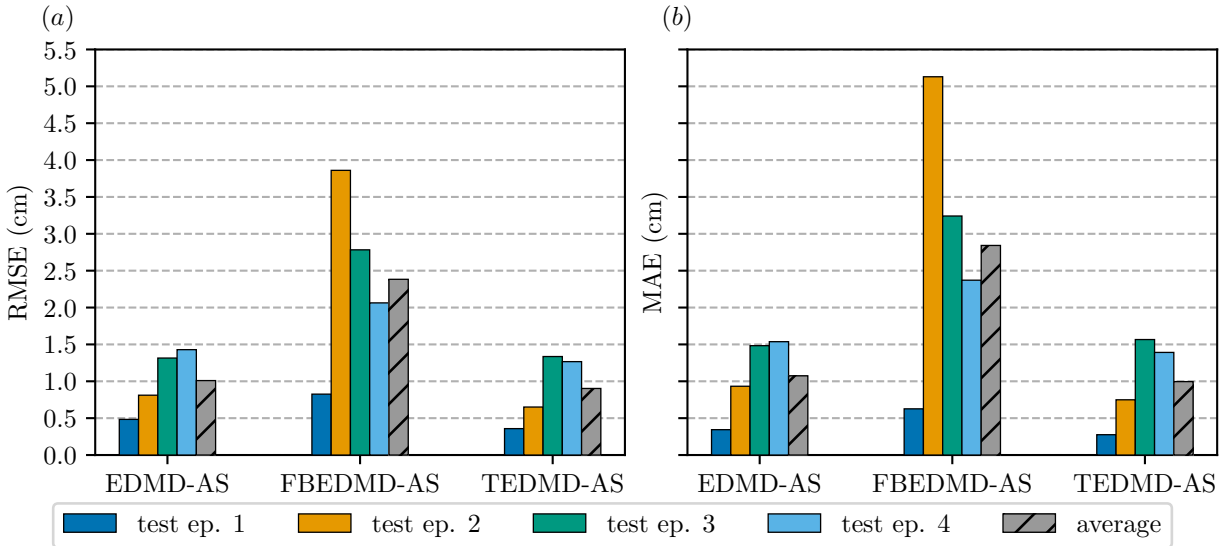


(ii) Prediction error plot (a) and multi-step trajectory (b) for Koopman matrices identified with an SNR of 18 dB. The trajectory generated by the Koopman matrix identified with fbEDMD-AS exhibits a large bias compared to EDMD-AS and TEDMD-AS. Both Koopman matrices computed with EDMD-AS and TEDMD-AS predict trajectories with similar errors.

Figure 4: Prediction error plots and multi-step trajectories of the second test episode for all three asymptotically stable Koopman systems identified with the experimental soft robot arm dataset at an SNR of (i) 28 dB and (ii) 18 dB. At each step of the prediction, the states are recovered and re-lifted. The prediction starts at $t_i = 0$ s and finishes at $t_f = 24.5$ s.



(i) The root-mean-square (RMS) (a) and mean (b) multi-step prediction errors for Koopman matrices identified with an SNR of 18 dB. The prediction obtained with TEDMD-AS has higher averaged RMS and mean errors than both EDMD-AS and fbEDMD-AS. EDMD-AS has a higher mean error, but a lower RMS error than fbEDMD-AS.



(ii) The root-mean-square (RMS) (a) and mean (b) multi-step prediction errors for Koopman matrices identified with an SNR of 18 dB. The prediction obtained with TEDMD-AS has lower averaged RMS and mean errors than both EDMD-AS and fbEDMD-AS. Forward-backward EDMD-AS has higher RMS and mean errors than both EDMD-AS and TEDMD-AS.

Figure 5: The root-mean-square (RMS) and mean multi-step prediction errors for Koopman matrices identified using the four test episodes given in the experimental soft robot arm dataset at an SNR of 28 dB (i) and 18 dB (ii).

The same experiment can be done when a greater amount of noise is added to the dataset. With an SNR of 18 dB, Figure 4ii shows that fbEDMD-AS does not perform well compared to EDMD-AS and TEDMD-AS. As explained in [21], when too much noise is present in the dataset, the high condition numbers of the snapshot matrices cause the relationships between the forward- and backward-in-time dynamics to hold approximately instead of exactly, leading to a poor performance of fbEDMD-AS. Again, the root-mean-square and mean errors are used, since the predicted trajectory of EDMD-AS and TEDMD-AS are too similar to decide which method performs better. In Figure 5ii, the predicted trajectory generated using TEDMD-AS has both a lower root-mean-square and mean error than EDMD-AS

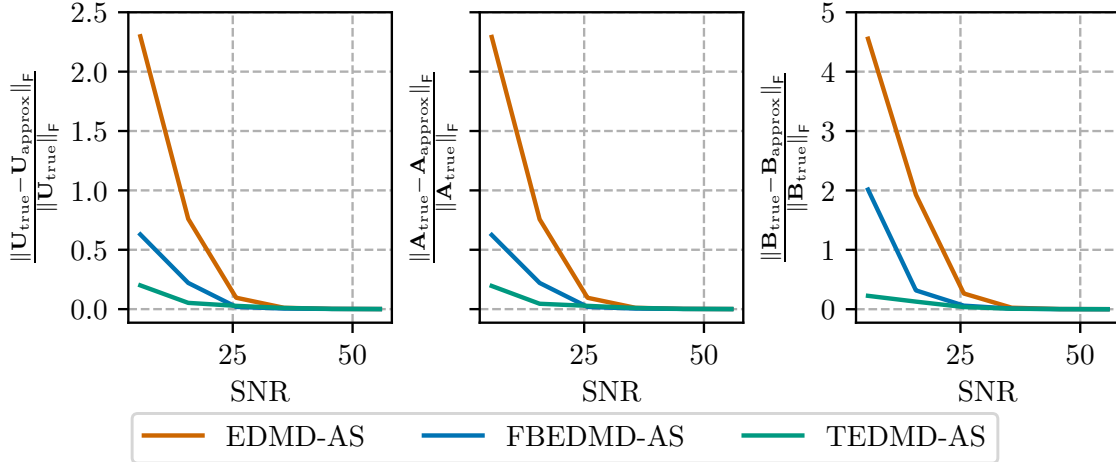


Figure 6: Relative error, using the Frobenius norm, between the approximated and true Koopman matrices, dynamics matrices, and input matrices at different SNRs. For all matrices computed with EDMD-AS, the relative error is greater than fbEDMD-AS and TEDMD-AS at all SNRs. Around an SNR of 25 dB, there is a threshold of added noise reached, where matrices computed with TEDMD-AS have a lower relative error than with fbEDMD-AS when more noise is added. At higher SNRs, fbEDMD-AS computes matrices with the lowest relative errors.

and fbEDMD-AS. From the results, TEDMD-AS performs better than both EDMD-AS and fbEDMD-AS in terms of trajectory prediction above a certain threshold of noise. As observed in Figure 5, the trajectory predicted with a Koopman matrix identified using TEDMD-AS has lower RMS and mean errors when more noise is present in the dataset. Note that this result is similar to the one obtained with the simulated Duffing oscillator dataset.

Considering that above a certain threshold of noise, TEDMD-AS identifies a Koopman matrix that predicts trajectories better than EDMD-AS and fbEDMD-AS with both the simulated and experimental datasets, it follows that the Koopman representation obtained with TEDMD-AS is more accurate than with EDMD-AS and fbEDMD-AS above a certain SNR. Note that for this section, the notion of accuracy is presented as a measure of proximity between the approximated Koopman matrix to the true Koopman matrix in terms of the Frobenius norm of the relative error. The approximated Koopman matrix is the Koopman matrix identified using the dataset with added noise and the true Koopman matrix is the Koopman matrix identified using the original dataset. In Figure 6, the approximated Koopman matrix identified with TEDMD-AS is more accurate than with EDMD-AS and fbEDMD-AS around an SNR of 25 dB and below. Above an SNR of approximately 25 dB, although the identified Koopman matrices with all methods share a similar accuracy, fbEDMD-AS is more accurate than both EDMD-AS and TEDMD-AS. The same result is not only observed in the dynamics matrix of Figure 6, but also in the input matrix, which indicates that the proposed adaptation of TDMD to TEDMD in Section 3.2 is valid.

From the results of this section, EDMD-AS is shown to be the best method for predicting trajectories when a low amount of noise is present in the dataset. However, TEDMD-AS is the preferred method when a higher amount of noise is present in the dataset. In terms of accuracy, when accuracy is defined as the Frobenius norm of the relative error between the approximated and true Koopman matrices, EDMD-AS always gives a less accurate Koopman matrix over all SNRs, while TEDMD-AS is the best method at low SNRs and fbEDMD-AS at high SNRs.

6 Conclusion

Obtaining a Koopman representation of a real system with data-driven methods in the presence of noise is a difficult task, since a biased model can result. Moreover, regardless of the lifting functions used, it's important that the approximate Koopman model be asymptotically stable when the underlying dynamical system is asymptotically stable. The method proposed by this paper, TDMD with inputs and an asymptotic stability constraint, identifies an asymptotically stable approximate Koopman system with reduced bias when noisy data is used in the identification process, regardless

of the lifting functions chosen. Using a simulated dataset of a Duffing oscillator and an experimental dataset of a soft robot arm, the proposed method is shown to compute a Koopman matrix that is closer to the noiseless solution and predicts a trajectory with a lower error than the state-of-the-art methods above a certain threshold of noise.

One limitation of this work is the requirement of truncation in the projection step of the proposed method in order to decrease the condition number. Future work will be focused on using regularization methods to better condition the least-squares problem instead of truncating singular values. The work developed in [22], which proposes the use of the \mathcal{H}_∞ norm as a regularizer to improve the conditioning of the Koopman approximation problem, could potentially be adapted to the TEDMD framework.

7 Funding

This work was supported by CIFAR, the Natural Sciences and Engineering Research Council of Canada (NSERC) discovery grants program, the Fonds de recherche du Québec – Nature et technologies (FRQNT), the Toyota Research Institute, the National Science Foundation Career Award (grant no. 1751093) and the Office of Naval Research (grant no. N00014-18-1-2575).

8 Data accessibility

All plots and datasets are accessible through the repository available at https://github.com/decargroup/total_extended_dmd_koopman.git.

9 Acknowledgements

The authors thank Steven Dahdah for providing meaningful insight that helped push this research project forward. The authors thank Daniel Bruder, Xun Fu and Ram Vasudevan for graciously providing the soft robot dataset used in this research.

References

- [1] Stephen A Billings. *Nonlinear system identification: NARMAX methods in the time, frequency, and spatio-temporal domains*. John Wiley & Sons, 2013.
- [2] J Nathan Kutz, Steven L Brunton, Bingni W Brunton, and Joshua L Proctor. *Dynamic mode decomposition: data-driven modeling of complex systems*. SIAM, 2016.
- [3] Steven L Brunton, Marko Budišić, Eurika Kaiser, and J Nathan Kutz. Modern Koopman theory for dynamical systems. *arXiv preprint arXiv:2102.12086*, 2021.
- [4] Alexandre Mauroy, Y Susuki, and I Mezić. *Koopman operator in systems and control*. Springer, 2020.
- [5] Steven L Brunton and J Nathan Kutz. *Data-driven science and engineering: Machine learning, dynamical systems, and control*. Cambridge University Press, 2022.
- [6] Jose Nathan Kutz. *Data-driven modeling & scientific computation: methods for complex systems & big data*. OUP Oxford, 2013.
- [7] Igor Mezić. Analysis of fluid flows via spectral properties of the Koopman operator. *Annu. Rev. Fluid Mech.*, 45:357–378, 2013.
- [8] Matthew O Williams, Ioannis G Kevrekidis, and Clarence W Rowley. A data-driven approximation of the Koopman operator: Extending dynamic mode decomposition. *J. Nonlinear Sci*, 25:1307–1346, 2015.
- [9] Milan Korda and Igor Mezić. Linear predictors for nonlinear dynamical systems: Koopman operator meets model predictive control. *Automatica*, 93:149–160, 2018.

- [10] Igor Mezić. Spectrum of the Koopman operator, spectral expansions in functional spaces, and state-space geometry. *J. Nonlinear Sci.*, 30(5):2091–2145, 2020.
- [11] Marko Budišić, Ryan Mohr, and Igor Mezić. Applied Koopmanism. *Chaos* 22, 22(4), 2012.
- [12] Peter J Schmid. Dynamic mode decomposition of numerical and experimental data. *Journal of fluid mechanics*, 656:5–28, 2010.
- [13] Joshua L Proctor, Steven L Brunton, and J Nathan Kutz. Dynamic mode decomposition with control. *SIAM J. Appl. Dyn. Syst.*, 15(1):142–161, 2016.
- [14] Milan Korda and Igor Mezić. Optimal construction of Koopman eigenfunctions for prediction and control. *IEEE Transactions on Automatic Control*, 65(12):5114–5129, 2020.
- [15] Alexandre Mauroy and Igor Mezić. Global stability analysis using the eigenfunctions of the Koopman operator. *IEEE Transactions on Automatic Control*, 61(11):3356–3369, 2016.
- [16] Daniel Bruder, Brent Gillespie, C David Remy, and Ram Vasudevan. Modeling and control of soft robots using the Koopman operator and model predictive control. In *Proc. Robot.: Sci. Syst. XV, Freiburg im Breisgau, Germany. RSS Foundation.*, 2019.
- [17] Daniel Bruder, Xun Fu, R Brent Gillespie, C David Remy, and Ram Vasudevan. Data-driven control of soft robots using Koopman operator theory. *IEEE Trans. Robot.*, 37(3):948–961, 2020.
- [18] Scott Dawson, Maziar S Hemati, Matthew O Williams, and Clarence W Rowley. Characterizing and correcting for the effect of sensor noise in the dynamic mode decomposition. *Exp. Fluids*, 57(3):1–19, 2016.
- [19] Maziar S Hemati, Clarence W Rowley, Eric A Deem, and Louis N Cattafesta. De-biasing the dynamic mode decomposition for applied Koopman spectral analysis of noisy datasets. *Theoretical and Computational Fluid Dynamics*, 31:349–368, 2017.
- [20] Gene H Golub and Charles F Van Loan. An analysis of the total least squares problem. *SIAM J. Numer. Anal.*, 17(6):883–893, 1980.
- [21] Louis Lortie, Steven Dahdah, and James Richard Forbes. Forward-backward extended DMD with an asymptotic stability constraint. *arXiv preprint arXiv:2403.10623*, 2024.
- [22] Steven Dahdah and James R Forbes. System norm regularization methods for Koopman operator approximation. *Proceedings of the Royal Society A*, 478(2265):20220162, 2022.
- [23] Ivan Markovsky and Sabine Van Huffel. Overview of total least-squares methods. *Signal processing*, 87(10):2283–2302, 2007.
- [24] Masih Haseli and Jorge Cortés. Approximating the Koopman operator using noisy data: noise-resilient extended dynamic mode decomposition. In *2019 Amer. Control Conf.*, pages 5499–5504. IEEE, 2019.
- [25] Amir Hossein Abolmasoumi, Marcos Netto, and Lamine Mili. Robust dynamic mode decomposition. *IEEE Access*, 10:65473–65484, 2022.
- [26] Giorgos Mamakoukas, Ian Abraham, and Todd D Murphey. Learning data-driven stable Koopman operators. *Free Radic. Niol. Med.*, 2020.
- [27] Steven Dahdah and James Richard Forbes. Linear matrix inequality approaches to Koopman operator approximation. *arXiv preprint arXiv:2102.03613*, 2021.
- [28] Mohamed A Mabrok, Ilyasse Aksikas, and Nader Meskin. Koopman operator approximation under negative imaginary constraints. *IEEE Control Syst. Lett.*, 2023.
- [29] Keita Hara, Masaki Inoue, and Noboru Sebe. Learning Koopman operator under dissipativity constraints. *IFAC-PapersOnLine*, 53(2):1169–1174, 2020.
- [30] Keita Hara and Masaki Inoue. Gain-preserving data-driven approximation of the Koopman operator and its application in robust controller design. *Mathematics*, 9(9):949, 2021.

- [31] Matan Gavish and David L Donoho. The optimal hard threshold for singular values is $4/\sqrt{3}$. *IEEE Trans. Inf. Theory*, 60(8):5040–5053, 2014.
- [32] Nick Vannieuwenhoven, Raf Vandebril, and Karl Meerbergen. A new truncation strategy for the higher-order singular value decomposition. *SIAM Journal on Scientific Computing*, 34(2):A1027–A1052, 2012.
- [33] Bert W Rust. *Truncating the singular value decomposition for ill-posed problems*. National Institute of Standards and Technology, 1998.
- [34] Katsuhiko Ogata. *Discrete-time control systems*. Prentice-Hall, Inc., 1995.
- [35] Ryan James Caverly and James Richard Forbes. LMI properties and applications in systems, stability, and control theory. *arXiv preprint arXiv:1903.08599*, 2019.
- [36] Steven Dahdah and James Richard Forbes. `decargroup/pykoop v1.2.3`. Zenodo, 2023. <https://doi.org/10.5281/zenodo.7464660>.
- [37] Timothy Sauer. *Numerical analysis*. Addison-Wesley Publishing Company, 2017.
- [38] Michael D McKay, Richard J Beckman, and William J Conover. A comparison of three methods for selecting values of input variables in the analysis of output from a computer code. *Technometrics*, 42(1):55–61, 2000.
- [39] V Eglajs and P Audze. New approach to the design of multifactor experiments. *Problems of Dynamics and Strengths*, 35(1):104–107, 1977.
- [40] Jun Qi, Jun Du, Sabato Marco Siniscalchi, Xiaoli Ma, and Chin-Hui Lee. On mean absolute error for deep neural network based vector-to-vector regression. *IEEE Signal Processing Letters*, 27:1485–1489, 2020.
- [41] Dulakshi Santhusitha Kumari Karunasingha. Root mean square error or mean absolute error? Use their ratio as well. *Information Sciences*, 585:609–629, 2022.